Sedimentology (1997) **44**, 1103–1113

Relations between dune morphology, air flow, and sediment flux on reversing dunes, Silver Peak, Nevada

C. McKENNA NEUMAN*§, N. LANCASTER† and W. G. NICKLING‡
**Department of Geography, Trent University, Peterborough, Ontario, Canada K9 J 7B8*
(E-mail: cmckneuman@trentu.ca)
†Desert Research Institute, University and Community College System of Nevada, Reno, USA
‡Department of Geography, University of Guelph, Guelph, Ontario, Canada N1G 2W1,
§Corresponding author

ABSTRACT

Relations between wind speed, sediment flux and dune morphology were measured for two reversing dunes situated in the south-western part of the Silver Peak dunefield in Clayton Valley, west-central Nevada. The larger dune was 120 m in length with a height of 12·5 m and the smaller dune 80 m long and 6 m high. Both dunes were sharp crested, aligned approximately E–W perpendicular to the dominant wind direction, and had slightly concave stoss profiles. Twenty-seven rotating cup anemometers were placed (0·3 m elevation) along N–S transects on each of the dunes. At each anemometer site a passive wedge-shaped sediment trap was used to measure sediment flux. Amplification of wind speed was observed towards the crest on the stoss side of both dunes with speed-up factors (u_{crest}/u_{base}) ranging from 1·50–3·19, with a corresponding increase in sediment flux by 1–2 orders of magnitude. In general, the ratio of crest flux to base flux (q_c/q_b) increased with increasing incident basal wind speed on both dunes. Direct measurements of the stoss slope variation in sediment flux relative to the dune crest are in good agreement with Owen's transport model. Friction speed ($u*$) was approximated from near surface (0·3 m) point wind speed. Although not all assumptions of the Owen model are upheld, the modified model performance is sufficiently robust to predict short-term variation in stoss sediment flux on the study dunes.

Improved models that adequately account for variation in sediment flux under changing air flow and transport conditions are necessary for the prediction of long-term evolution of dunes. In this regard, further progress in model development will require increased understanding of the spatial and temporal variability of airflow and the short term response of sediment flux to these flow conditions.

INTRODUCTION

The morphology of desert sand dunes is determined by interactions between the bedform, airflow and sediment flux. Dunes cause flow convergence in the atmospheric boundary layer so that the imbalance in pressure force is manifested in flow acceleration and rising boundary shear stress (τ_0) along the stoss slope towards the crest. On the lee side, flow expansion and increasing pressure can lead to a variety of secondary flow patterns. Changes in wind friction speed ($u*$) give rise to variations in sediment transport rates through time and space that result in erosion or deposition of sediment through the principle of sediment continuity (Middleton & Southard, 1984). Patterns of erosion and deposition ultimately determine dune morphology.

In this paper, we examine these interactions using field studies of two-dimensional airflow

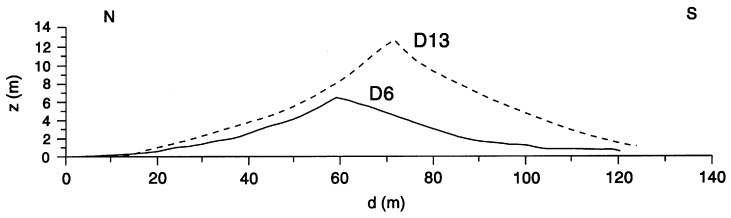

Fig. 1. Surveyed profiles of the two study dunes, D6 and D13. Vertical exaggeration factor is 2.

and sediment transport on reversing dunes with different slope angles and aspect ratios at Silver Peak, Nevada. Based on previous work (Frank & Kocurek, 1996; Lancaster *et al.*, 1996), we abandoned wind profile measurements in favour of spatially detailed wind speed measurements at a single height ($z = 0{\cdot}3$ m) within the inner boundary layer. Friction speed was obtained from a logarithmic model of the wind speed profile which incorporated Owen's (1964) modification for roughness effects associated with mass transport. Direct measurements of along-slope variation in q are used to evaluate the extension of several sediment flux models (Kawamura, 1951; Owen, 1964; Lettau & Lettau, 1978) to inclined surfaces.

STUDY SITES

Two study dunes (hereafter referred to by their respective heights as D6 and D13) were selected to represent a range of dune height (h) and slope angle (θ) (Fig. 1). Both dunes were near-symmetrical, E–W trending reversing ridges situated in the south-western part of the Silver Peak dunefield in Clayton Valley, west-central Nevada. D6 was 80 m long and 6·12 m high with a sharp crest aligned transverse to the prevailing north and south winds. A 3·7 m high dune of similar shape was located 80 m to the north of D6, while a 4·1 m high reversing ridge lay 140 m to the south. During the period of study on D6 (May, 1994), the winds reversed direction from northerly to southerly on several occasions so that the orientation and height of the lee face changed. Maximum lee face height was 1·5 m, orientated to the south. In comparison, the sharply defined crestline of D13 was 12·5 m above the interdune which separated it from a 5 m high rounded-crest reversing dune 140 m to the north. Dune length was 120 m. Winds during the period of study on D13 (early June, 1995) were from the north, resulting in a south-facing slip face 2·5 m high. Both dunes had a slightly concave profile and consisted of a plinth area with slopes of 5–8° steepening toward the crest to 9–14·5°. D13 was steeper than D6, with an aspect ratio of 0·22 as compared to 0·11. The dunes were composed of moderately sorted medium sands (mean size = 300–500 μm) with particle density of 2540 kgm^{-3} and a shape factor averaging 0·77 (circle = 1; line = 0).

INFLUENCE OF TERRAIN ON NEAR-SURFACE WINDS

Recent studies (e.g. Wiggs, 1993; Frank & Kocurek, 1996; Lancaster *et al.*, 1996) have highlighted the problem of derivation of friction speed ($u*$) from wind profile measurements on dune stoss slopes. For example, several of these researchers have calculated a decrease in $u*$ up the stoss slope despite measured *increases* in sediment flux (q) and wind speed (u_z). This suggests that the wind profiles measured in these studies did not lie within the inner part of the boundary layer responsible for the transport of sediment.

Air flow over dunes can be represented in a similar way to flow over low hills, using analytical models of turbulent flow such as those described in Jackson & Hunt (1975) and Hunt *et al.* (1988), the linear mixed spectral finite difference model (MSFD) of Beljaars *et al.* (1987), and its non-linear extension (NLMSFD) (Xu & Taylor, 1992).

A generalized presentation of Taylor & Gent's (1974) analytical model of the variation in surface pressure and surface shear stress over a 'standard' hill (height 500 z_0, length 10^4 z_0) is shown in Fig. 2b. Although more sophisticated models now exist, the essential qualitative features remain unchanged from this early work. As the airflow approaches the hill, it first induces a rise in pressure on the stoss face because of a stagnation effect. Acceleration over the top of the hill leads to a very low pressure at the crest prior to recovery on the lee face. The variation in surface shear stress is the inverse of the pressure variation with distance. In comparison to incident values, shear stress magnitude is depressed

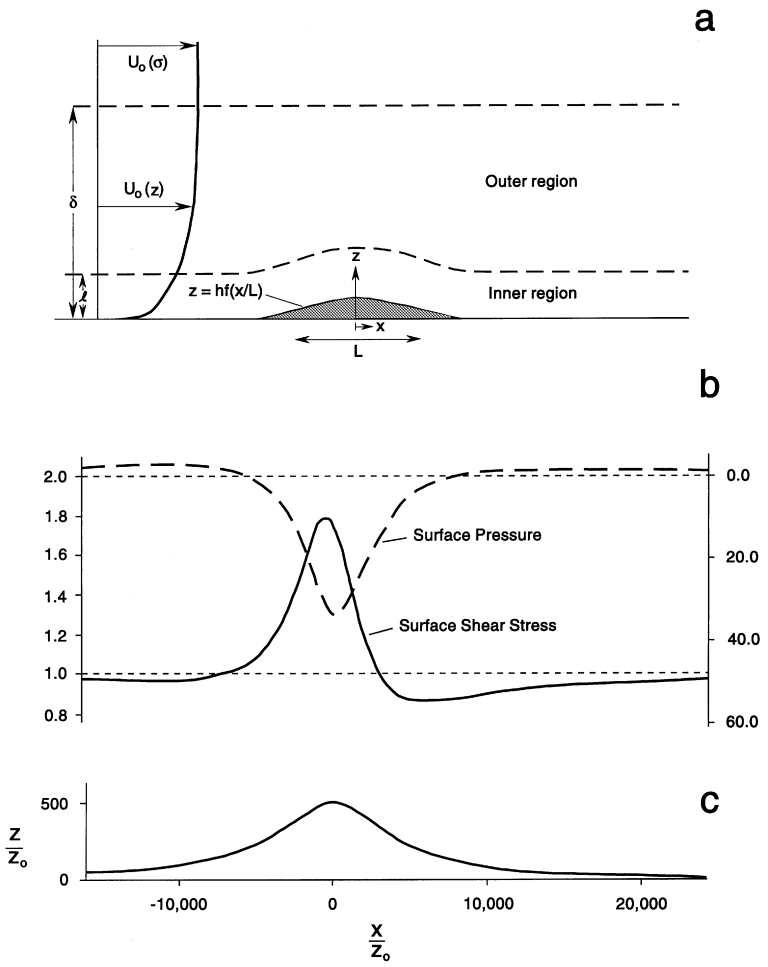

Fig. 2. (a) The boundary layer over a low hill (after Jackson & Hunt, 1975). (b) Analytical model of variations in surface shear stress and pressure over a 'standard' hill (after Taylor & Gent, 1974). (c) Hill morphology with length and height expressed in dimensionless form.

slightly on the lower stoss slope. From a point which has an elevation roughly half the hill height, surface shear stress increases dramatically. On gently sloping hills, Jackson & Hunt (1975) suggest that the surface shear stress is doubled at the hill crest.

Models of wind flow over hills frequently divide the boundary layer depth (δ) into outer and inner regions (Fig. 2a). Within the inner region, the wind speed profile is approximately logarithmic. Following Jackson & Hunt (1975), the inner layer thickness (l) can be computed from:

$$l/\mathrm{L}\ln(l/z_0) = 2\kappa^2 \qquad (1)$$

where L is a horizontal length scale, in this case the distance from the dune crest to the point where the elevation is half its maximum (Hunt, 1980). Von Karman's constant is represented as κ, and the roughness length as z_0. The inner boundary layer thickness for D13 and D6 computed from Eq. (1) was 1·16 m and 0·94 m, respectively, with $z_0 = 0{\cdot}00008$ m, L(D13) = 28 m and L(D6) = 22 m as determined from direct measurement. This inner portion of the boundary layer can be subdivided into two further sublayers: the shear stress layer and an inner surface layer of thickness $l_s \approx (lz_0)^{0.5}$ (Hunt *et al.*, 1988). It is only within the inner surface layer that shear stress is strictly constant and in equilibrium with the underlying bed roughness. The thickness of this layer (l_s) is ≈ 1 cm for the Silver Peak study dunes.

In hill flow models, such as those cited above, the surface is assumed to be immobile and spatially homogeneous. Where the surface is comprised of loose, transportable grains, the flow within the inner stress layer will only be in equilibrium with the surface conditions if the bed remains immobile (i.e z_0 remains constant). Owen (1964), on theoretical grounds, has demonstrated that the transport of sediment in saltation causes an effective increase in the surface roughness that varies proportionally with mass transport, which is in turn a function of the friction speed ($u*$)

above the saltation threshold ($u*_t$). He suggests that the dependency of z_0 on mass flux can be estimated from:

$$(u_*^2/2g) \sim z_0 \quad (2)$$

Consequently, modelling of flow over dunes must account for the changes in surface roughness attributed to sediment transport which will vary up-slope as $u*$ changes.

The predicted up-slope changes in pressure, surface shear stress and bed roughness have significant ramifications for sediment transport on dunes. On a given stoss slope where the wind is sufficiently strong that the boundary layer is fully saturated with grains, a doubling of shear stress would indicate an increase in sediment transport at the crest by a factor of 2·8 relative to the base (i.e. $q \propto u*^3$). In lighter winds where the lower portions of the slope are not fully mobile, this factor may be orders of magnitude higher. Also, the very presence of grains in the lower atmosphere causes an apparent increase in surface roughness which alters the near surface wind profile. This then alters the surface shear stress and in return sediment entrainment. These feedback mechanisms make modelling of sediment transport extremely complex. Because surface shear stress can not be measured directly, it must be estimated from the near surface wind profile that changes up the dune. A method for approximating changes in up-slope surface shear stress, based on near surface wind speeds ($z = 0{\cdot}3$ m), is presented in this paper and compared to direct measurements of the sediment flux along the stoss slopes of the two study dunes.

INSTRUMENTATION AND METHODS

Rotating cup anemometers (R.M. Young, Wind Sentry model) were placed as close to the surface as possible ($z = 0{\cdot}3$ m) without interference, and well within the inner boundary layer, at 4 m horizontal intervals along straight N–S transects orientated perpendicular to the alignment of the dune crests (Fig. 3). The smaller dune (D6) was instrumented in May 1994 and the larger one (D13) in June 1995. Three wind direction vanes were placed also at $z = 0{\cdot}3$ m on each slope (north and south orientations); one near the dune crest, one midslope and one at the dune toe. During periods when there was transport of sediment on the dune surface, wind speed was sampled every second and averaged over a one minute period.

A passive, wedge shaped sediment trap (Nickling & McKenna Neuman, 1997) was installed at each anemometer site. In order to reduce flow interference, the position of these traps alternated to the east and west of the anemometer transect by 1·5–2 m. The base of each trap was dropped into an oversized section of PVC tubing (diameter 0·10 m, length 0·20 m) which was buried in the dune surface to provide a fixed trap position. The trap intake nozzle was aligned perpendicular to the orientation of the local ripple crests on the dune surface, and approximately parallel to the local airflow. An entrance lip prevented scour around the trap nozzle while the sand surface was stabilized by light wetting within 0·2 m of the trap sides and rear. The collection period (typically 10–20 min) ended when the traps at the crest were filled to capacity (≈ 1200 g). All runs began

Fig. 3. View of typical array of anemometers and sand traps on a study dune (D13, north slope).

with the removal of a sponge bung from the trap nozzle and ended with its replacement. Each trap was then lifted from the in-ground cowling. The plastic bag containing the captured sand was removed, reserved for later weighing, and replaced with a new bag for the next run.

RESULTS

Airflow over the study dunes

Figure 4 shows examples of the stoss-side wind speed amplification toward the crest on each of the two dunes. One minute averages of wind speed at the dune crests ranged between 6·4 and 15·4 ms^{-1}. The speed-up ratio (u_c/u_b) generally fell within the range 1·5–2 (Table 1), depending on the morphology of the reversing dune crest at the time of sampling. These values are very similar to those measured elsewhere (Lancaster, 1995). The highest speed-up factor (3·19) describes a situation in which the wind direction switched directly from north to south so that the dune morphology was out of equilibrium with the new flow direction. Reworking of a former slipface as a stoss slope is associated with very steep gradients, and therefore, large speed-up within several meters of the crests of these reversing dunes.

As a general rule, wind speed on the north slopes of D6 and D13 (Fig. 4a,c) increased by only a small amount ($< 1{\cdot}5\ ms^{-1}$) for $0 \le d/D \le 0{\cdot}8$, where d is the horizontal distance from the dune base, and D is the horizontal length of the stoss slope. In the upper 20% of the stoss slope ($0{\cdot}8 \le d/D \le 1$), $u_{0\cdot3}$ rose sharply with distance by 4–6 ms^{-1}. A more consistent and gradual increase in $u_{0\cdot3}$ generally was observed on the south facing stoss slope of D6 (Fig. 4b). The stagnation effect is evident in the comparatively small increase in wind speed on the lowest portions of all three stoss slopes. This effect may have been influenced also by pressure disturbances associated with the presence of the upwind transverse ridges.

Near surface return flow in opposition to the direction of the main windward flow was common along the slip face of all dunes. The fractional drop in wind speed beyond the brink of D13 was greater than on D6, with $u_{0\cdot3}$ returning to windward levels within 15–20 m of the crest, as compared to only 2–4 m for D6. This was likely a result of the higher aspect ratio of D13 which forced a greater degree of flow separation in the manner suggested by Sweet & Kocurek (1990).

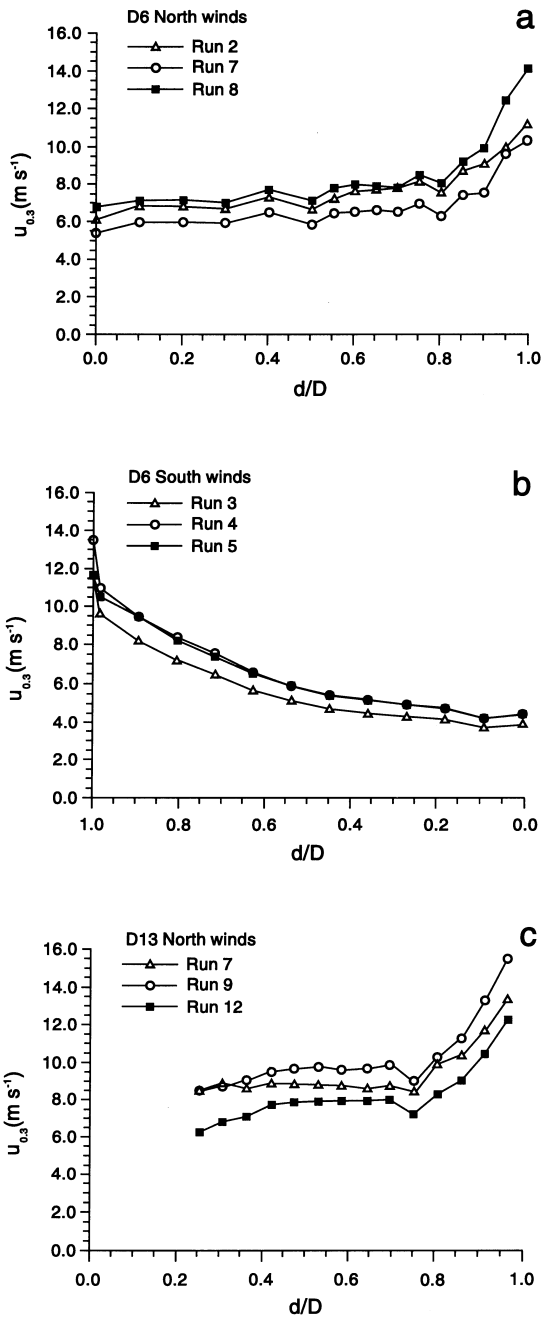

Fig. 4. Typical variation in wind speed at 0·3 m on the stoss slope of D6: (a) north winds (b) south winds, and on D13: (c) north winds.

Relations between sediment flux and wind speed

A positive relation is observed between sediment flux (q) and wind speed ($u_{0\cdot3}$) as shown in Fig. 5, based on data from six sampling runs for D13, five runs for D6-N and three runs for D6-S. Wind speed generally exceeded 9 ms^{-1} in the 1995 data set for D13, which corresponded to a single large magnitude event. In the previous year, there was

Table 1. Speed-up factor given as the ratio of wind speed at the dune crest (u_c) to that at the base of the dune (u_b).

Run	Speedup Factor	
	N	S
D6	1·5	
	1·81	
		3·03
		3·19
	1·91	
	2·08	
	2·09	
D13	1·96	
	1·56	
	1·56	
	1·83	
	1·78	
	1·79	
	1·95	

a greater range in wind speed magnitude (4–16 ms^{-1}) collected over a number of days on D6. Nonetheless, there is a clear continuum between the data sets which collectively indicate that q is strongly correlated with wind speed amplification on stoss slopes. As a strictly empirical guideline, the power function $q \sim u_{0\cdot3}{}^n$ where $n = 5\cdot6$ does appear to describe the data set well ($r^2 = 0\cdot91$) for $u_{0\cdot3} > 6$ ms^{-1}. However, physical reasoning does not justify the use of a single value for the exponent n, as it is widely recognized that the influence of the transport stage $u*_t/u*$ on q is very significant near the threshold of motion, but can be neglected at high wind speeds so that $q \propto u*^3$. The south slope of D6 appears to have had a lower threshold for grain motion ($u_t \approx 4$ ms^{-1}) than the north slope ($u_t \approx 6$ ms^{-1}). This could be attributed to the reworking of relatively fine and loosely packed grainfall deposits formed under a preceding north wind event.

Unfortunately, direct measurement of q is impractical to carry out on a long-term basis, and thereby cannot represent the full range of temporal variability in dune dynamics. Modelling of sediment flux–wind field relations, therefore, is necessary for development of dune form–sediment transport relations.

For the purpose of evaluating the extension of conventional horizontal-bed sediment transport models to inclined surfaces, estimates of $u*$ were calculated iteratively from $\kappa u_z/u_* = \ln(2gz/u_*^2) + C$, assuming the wind profile in the inner boundary layer of the dunes is logarithmic, as suggested by the model of Hunt (1980). In this specific expression, which Owen (1964) introduced as a variation on the Prandtl equation, the roughness associated with mass transport is accommodated in the term $(u*^2/2\ g) \sim z_0$. A value of 6·2 was determined for the empirical coefficient C from wind profiles measured within 2 m of an open, level surface near the D6 site. This value is lower than C = 9·7 which Owen (1964) established from his wind tunnel studies. Rasmussen *et al.* (1996) also found in sloping wind tunnel studies that this coefficient is not constant as Owen

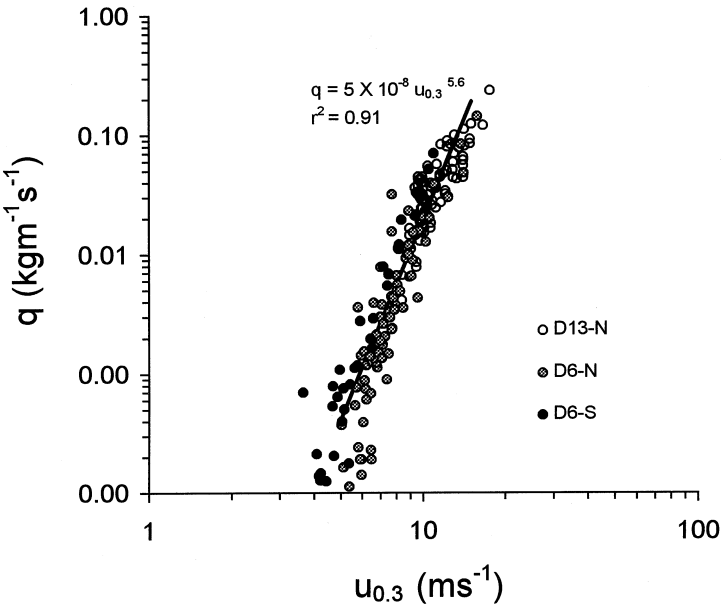

Fig. 5. Relation between measured sediment flux (q) and wind speed ($u_{0\cdot3}$).

suggested, but demonstrates some dependency on grain size and friction speed. Slope angle, however, was not found to affect the value of C.

In order to compute exact estimates of u_* from $u_{0\cdot3}$, the shear stress at 0·3 m would have to be the same as that within the 1 cm thick inner surface layer on these dunes. As neither this assumption nor the validity of Owen's roughness expression was tested directly in this field study, the absolute values reported for u_* are not definitive. However, they do provide useful insight on the relative differences in friction speed along the stoss slopes studied.

Threshold friction speed (u_{*t0}, horizontal surface) was determined from examination of transport data. As the base of each dune occasionally was not active, it was possible to establish the point along the instrumented transect at which transport started, $u_{0\cdot3}$ at this location indicating u_{*t0}. From examination of all data runs, u_{*t0} was estimated at 0·28 ms^{-1} for D6-N and D13, and 0·21 ms^{-1} for D6-S. These thresholds were adjusted to account for the influence of slope angle (θ) using the relation suggested by Iversen & Rasmussen (1994)

$$\frac{u_{*t}^2}{u_{*t0}^2} = \frac{\sin\theta}{\tan\alpha} + \cos\theta \qquad (3)$$

where α is the angle of repose in the absence of inter-particle force (taken here as 34°). The maximum correction factor on D13 was 1·26 and 1·16 on D6.

Figure 6 shows the estimated influence of the transport stage ratio (u_*/u_{*t}) on the dimensionless sediment flux ($qg/\rho u_*^3$) for the three stoss slopes studied at the Silver Peak dune field. As expected, the dimensionless flux drops to very low values as the transport stage approaches unity. The saltation layer was rarely saturated with grains, which by Maegley's (1976) definition occurs when $u_* \approx 3u_{*t}$. With the stronger winds in 1995 as compared to 1994, it appears that threshold had relatively little influence on the dimensionless flux measurements for D13 as compared to those for D6.

The considerable scatter in the plot in Fig. 6 may be attributed to a number of factors relating to the collection of the flux data, apart from the uncertainty regarding friction speed. Fluctuating collection efficiency associated with varied trap alignment into the airstream (Nickling & McKenna Neuman, 1997) was unavoidable. Organization of the mobile sediment into discrete sand streamers presented additional under-sampling problems for the array of narrow, vertical sediment traps installed in this study. Time averaging ($8 < \Delta t < 20$ min) of flux data introduces further measurement bias, given that wind gusting contributes most of the material caught in a trap. This bias was particularly evident for traps located low on a given slope, where the mean friction speed was often below threshold but the traps were never found empty of sediment. Scouring around the orifices of traps near the dune crests was sometimes observed at very high windspeeds, which also contributed to under-collection.

Therefore, it is obvious that when various physically based sediment flux relations are superimposed on the plot in Fig. 6, the values of

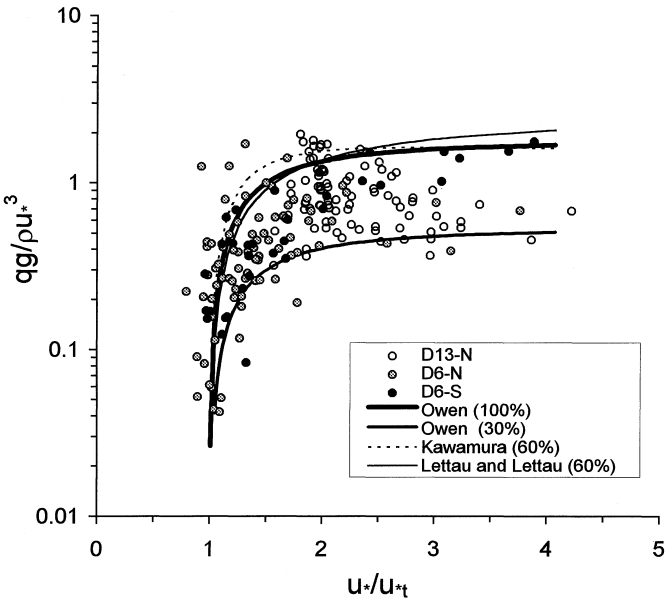

Fig. 6. Relations between transport stage and dimensionless sediment flux. Symbols refer to measurements from the Silver Peak dunes. Percentages of the typical values cited for the empirical coefficient (C′) in Table 2 are listed in the legend for each of the transport equations overlain on the plot.

Table 2. Sediment flux equations.

Source	Expression	C′
Owen (1964)	$qg/\rho u_*^3 = C'(1-u_{*t}^2/u_*^2)$	1·8 (3)
Kawamura (1951)	$qg/\rho u_*^3 = C'(1 + u_{*t}^2/u_*^2)(1-u_{*t}/u_*)$	2·3 (4)
Lettau and Lettau (1978)	$qg/\rho u_*^3 = C'(1-u_{*t}/u_*)$	4·2 (5)

the empirical coefficients reported from wind tunnel simulation (Table 2) must be reduced significantly to overlie the data set. Given that the trap efficiency was likely well below 100% during sampling in this study, most transport models will *appear* to over predict q. Even when the empirical coefficients in the models of Kawamura (1951), and Lettau & Lettau (1978) are dropped to 60% of their usual reported range, these relations fall just along the upper boundary of the data set. Owen's (1964) model seems to perform best, outlining the trend of the highest dimensionless fluxes with an unaltered empirical coefficient (i.e. $C' = 1{\cdot}8$, essentially a trap efficiency of 100% is assumed). However, extremely low values in the data set appear to represent a collection efficiency of only 30% as indicated by Owen's relation.

The flaw in this argument is that a lower than expected dimensionless flux could also be attributed to overestimation of the actual friction speed, which becomes even more influential when u_* is cubed. There is some evidence for this effect in the data for D13-N wherein the dimensionless flux appears to drop slightly as u_*/u_{*t} increases beyond 2·5. This drop is not observed if constant roughness along the stoss slope is assumed, suggesting that Owen's roughness term ($u_*^2/2\,g$) may overestimate the effect of saltation on boundary layer shear stress in this example. However, the same trend is not apparent in the D6-S data, which is well described by Owen's transport relation with an assumed moderate-high trap efficiency throughout the entire range of wind speed.

Spatial patterns of sediment flux

Examples of the typical variation in sediment flux measured for different wind events, but at the same sampling points, along surveyed transects of D6 and D13 are presented in Figs 7 and 8. While the increase in flux (q) with distance (d/D) on dune stoss slopes is suggestive of a relationship between q and local bed elevation, as surmised by some models of bedform development (e.g. Fredsoe, 1986), the family of power functions shown in Fig. 7 clearly indicates that no single, general relation can adequately describe all possible transport situations. In 1994, the sediment flux along ≈75% of the base-crest distance on D6 was under 10% of that at the crest (Fig. 8a,b). In comparison, the magnitude of the sediment

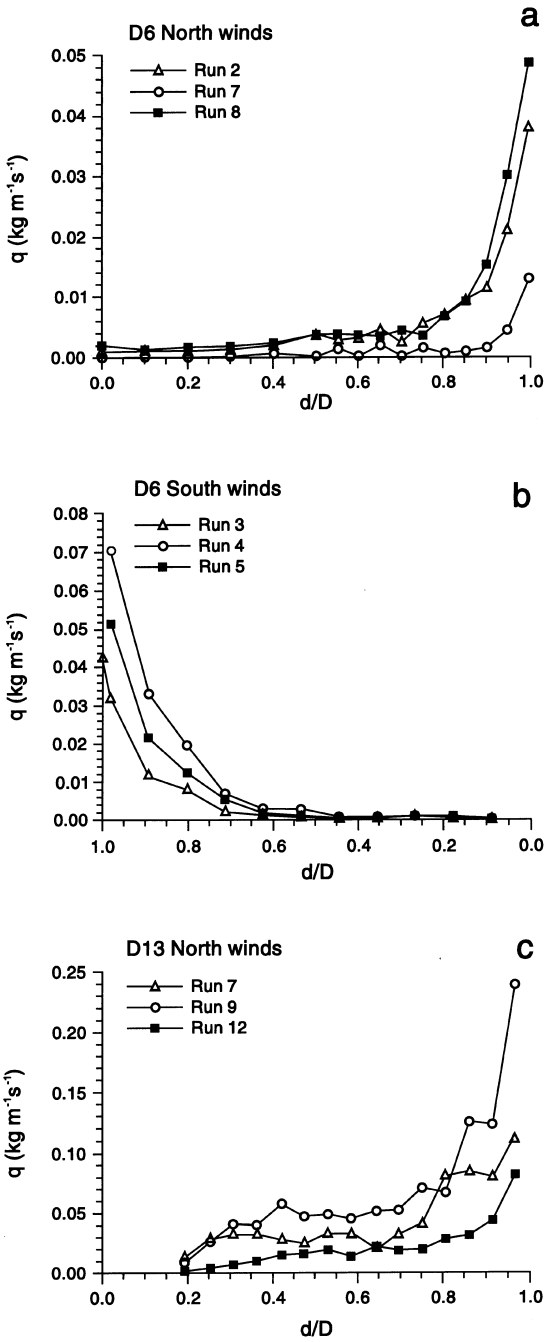

Fig. 7. Typical variation in sediment flux on the stoss slopes of D6: (a) north winds (b) south winds; and on the stoss slope of D13: (c) north winds.

transport rate relative to the crest (q/q_c) was marginally higher on D13 in 1995, varying between 10 and 35% for $d/D < 0{\cdot}75$ (Fig. 8c). The maximum flux measured within the duration of the study was 0·24 $kgm^{-1}s^{-1}$ at the crest of D13 in Run 9 (Fig. 8c). An inflection point in each of the flux vs. distance curves falls within $0{\cdot}6 < d/D < 0{\cdot}8$, whereupon the transport of sediment increased sharply by 70–90% in the area of the dune crest. As a general rule, the ratio of the flux at the stoss slope crest to that at the base (q_c/q_b) decreased as the incident wind speed (measured at the base of the slope) increased, indicating that sediment transport on the dune became more uniform when $u*_b/u*_t >> 1$.

Figure 8a–c reinforces the earlier observation that the up-slope amplification in $u_{0{\cdot}3}$, and thereby friction speed $u*$, drives the spatial variation in q. In each of the three sample runs shown, the trend in $u*^3$ is normalized by that at the dune crest, the transport stage is represented as $u*/u*_t$, and the product $u*^3\ (1-u*_t{}^2/u*^2)$ in Owen's transport equation provides the basis of a model estimate for q/q_c. The plots shown represent considerable variation in the threshold of particle motion, distance of sediment transport

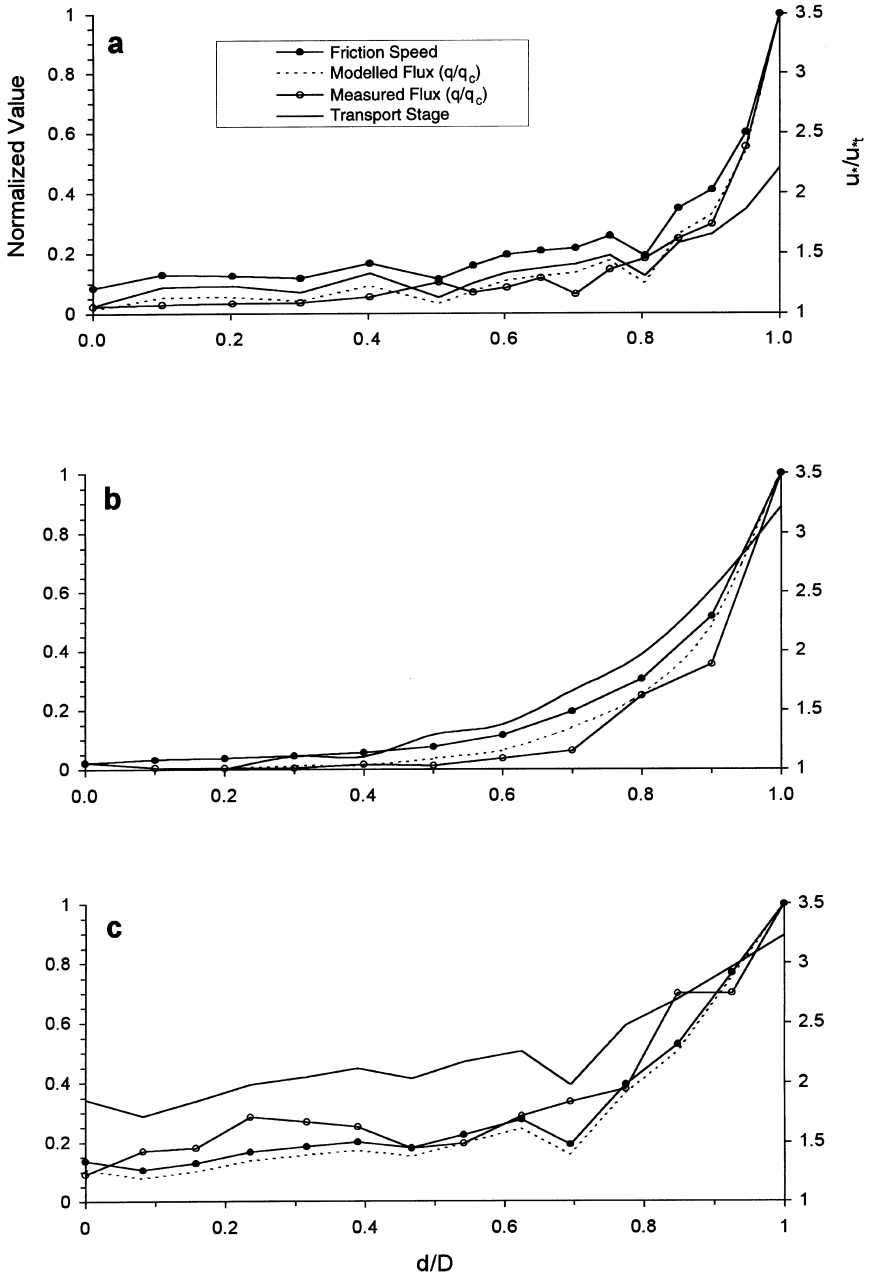

Fig. 8. Stoss slope variation in normalized friction speed ($u*^3/u*_c{}^3$) and sediment flux (q/q_c); values are plotted along the primary vertical axis. The influence of the transport stage is represented by the solid line as the ratio $u*/u*_t$ (secondary vertical axis). The model estimate for q/q_c, based on Owen's (1964) transport equation, is shown as the dashed line. Plots a–c indicate separate sample runs: (a) D6-N, Run 2; (b) D6-S, Run 3; and (c) D13-N, Run 9.

and incident air flow. These factors control the change in sediment flux with distance along the stoss slope.

In the case of Fig. 8b, D6-S was the shortest slope (D = 30 m) with the lowest incident wind speed ($u_b \approx 4$ ms^{-1}). Threshold friction speed played a key role in determining spatial variations in q. The lowest 1/3 of the south face of this dune was only intermittently mobile ($u*/u*_t \leq 1$) at the time of Run 3. Above and beyond this point, friction speed and the transport stage factor $u*/u*_t$ appear to have increased smoothly, reaching magnitudes of 0·56 ms^{-1} and 3·2, respectively, at the dune crest. The ratio of q_c to the flux at the base (q_b) was extraordinarily large at 550 as a result of the intensive reworking of the former slipface relative to the mostly stable dune base. In terms of the general variation in q/q_c with distance, the agreement between the modelled and measured values is reasonably good, with the modelled dimensionless flux slightly over estimating the measured values. The apparent prevalence of the stagnation effect in $u*^3/u*_c{}^3$ over the distance $d/D < 0{\cdot}5$ ($x/L > 1$) is also in good agreement with Jackson and Hunt's (1975) predicted variation in the normalized shear stress perturbation over a standard hill.

In the case of D13 (Fig. 8c), the incident windspeed averaged 9·5 ms^{-1} at the base of this 50 m slope. The transport stage factor $u*/u*_t$ increased from 2 to 3·2 along the incline, indicating that the saltation layer was well developed and close to saturation over much of this distance. Estimated friction speed at the crest of the dune reached 1·1 ms^{-1}. Because of the relatively uniform transport stage, q_c exceeded q_b by a factor of 9 as compared to the two orders of magnitude change observed for D6-S (Fig. 8b). In terms of upslope variation in q/q_c, the agreement between the modelled and sampled relations is also reasonably good with some bias toward under-estimation, particularly on the lower portion of the slope. In this example, the friction speed and flux curves lie very close to one another, indicating the dominance of $u*^3$, and thereby, the lesser influence of the threshold condition.

Figure 8a shows that the 40 m slope on D6-N ($u_b \approx 6$ ms^{-1}) represents a situation where the observed amplification in windspeed and sediment transport fell somewhere in between that described for the other two stoss slopes. As expected, there is greater separation between the friction speed and flux curves because of the significance of the transport stage factor. There continues to be good agreement between the variation in the dimensionless flux and the model estimates.

In working with flux measurements in the dimensionless form q/q_c, the apparent model success may be attributed in part to the elimination of the coefficient C′ (Table 2), so that while there is a good match in relative terms, this is not necessarily true in absolute terms. The suggested relation between C′ and trap collection efficiency was addressed above. It is further possible that this empirical coefficient may incorporate a number of incline-related transport processes not directly accounted for. Nonetheless, it is the spatial variation in transport which governs dune form, and therefore, the model performance is encouraging.

CONCLUSIONS

Our field measurements of wind speed and sediment flux on the windward slopes of reversing dunes show that flow acceleration up the dune gives rise to an increase in sediment transport toward the crest, by 1–2 orders of magnitude, so that the crest areas are most active. Accelerating flow and under-saturation of grains in the saltation layer means that in all cases erosion was occurring all along the windward slopes, wherever threshold was exceeded, with the amount of surface lowering increasing sharply at $d/D > 0{\cdot}8$ or $x/L < 0{\cdot}5$. Over time in a unidirectional wind this would lead to a flattening out of the feature.

Dunes subjected to bi-directional wind regimes (e.g. reversing dunes, star dunes, and many linear dunes) tend to have sharp crestlines and a triangular cross section, rather than the convex form of the crest common to most transverse flow dunes (Tsoar, 1985). The triangular profile is the result of the processes discussed above operating from two directions such that, at a given season, each profile will tend towards a convex form as it adjusts to that wind direction and its spectrum of wind velocities. The high rates of sediment flux, erosion and deposition observed in the crestal areas of the study dunes are a reflection of the process of adjustment to changing wind directions.

Field studies of dune dynamics are time consuming, expensive to carry out, and sample short time periods on the scale of minutes. Models of the behaviour of dunes under varied air flow and transport conditions are necessary therefore to be able to predict the long term evolution of dunes.

While a number of model assumptions are not strictly upheld in the present field application at the Silver Peak dune site, transport model performance, based on simple single level wind speed measurement, seems sufficiently robust to mimic the gross variation in sediment flux along the three stoss slopes. Further progress in model development will require additional information on the temporal variability in airflow and sediment transport adjustment, as well as refinements in flux monitoring technique.

ACKNOWLEDGMENTS

Funding for Nickling and McKenna Neuman was provided by grants from the Natural Science and Engineering Research Council, Canada; and from the Geological Society of America (Gladys W. Cole Research Award) for Lancaster. We thank Val Wyatt, Wayne Boulton, Paul Grant, Steve Metzger, Marley Murphy, and Marianne Maljaars for their assistance in the field. K. Rasmussen and G. Kocurek provided helpful comments on an earlier draft of this manuscript.

REFERENCES

Bagnold, R.A. (1973) The nature of saltation and 'bed-load' transport in water. *Proc. Roy. Soc. London*, **A332**, 473–504.

Beljaars, A.C.M., Walmsley, J.L. and Taylor, P.A. (1987) A mixed spectral finite-difference model for neutrally stratified boundary-layer flow over roughness changes and topography. *Boundary-Layer Meteor.*, **38,** 273–303.

Frank, A. and Kocurek, G. (1996) Airflow up the stoss slope of sand dunes: limitations of current understanding. *Geomorphology*, **17**(1–3), 47–54.

Fredsoe, J. (1986) Shape and dimensions of dunes in open channel flow. In: *Physics of Desertification* (Ed. by F. El-Baz and M. H. A. Hassan). Martinus Nyhoff, Dordrecht.

Hunt, J.C.R. (1980) *Wind over Hills: a Numerical Approach*. Workshop on the Planetary Boundary Layer. American Meteorological Society, Boston, 107–144.

Hunt, J.C.R., Leibovich, S. and Richards, K.J. (1988) Turbulent shear flows over low hills. *Quarterly J. Roy. Meteor. Soc.*, **114,** 1435–1470.

Iversen, J.D. and Rasmussen, K.R. (1994) The effect of surface slope on saltation threshold. *Sedimentology*, **41,** 721–728.

Jackson, P.S. and Hunt, J.C.R. (1975) Turbulent wind flow over a low hill. *Quarterly J. Roy. Meteor. Soc.*, **101,** 929–955.

Kawamura, R. (1951) *Study of sand movement by wind*. Institute of Science and Technology, Tokyo. pp. 95–112. Report **5,** Tokyo, Japan.

Lancaster, N. (1995) *Geomorphology of Desert Dunes*. Routledge, London.

Lancaster, N., Nickling, W.G., McKenna Neuman, C.K. and Wyatt, V.E. (1996) Sediment flux and airflow on the stoss slope of a barchan dune. *Geomorphology*, **17**(1–3), 55–62.

Lettau, K. and Lettau, H.H. (1978) Experimental and micro-meteorological field studies on dune migration. In: *Exploring the World's Driest Climate* (Ed. by K. Lettau and H. H. Lettau), pp. 110–147. Institute for Environmental Studies, University of Wisconsin-Madison.

Maegley, W.J. (1976) Saltation and martian sandstorms. *Rev. Geophys. Space Physics*, **14,** 135–142.

Middleton, G.V. and Southard, J.B. (1984) *Mechanics of Sediment Movement*. Society of Economic Paleontologists and Mineralogists, Tulsa, Oklahoma.

Nickling, W.G. and McKenna Neuman, C. (1997) Wind tunnel evaluation of a wedge-shaped aeolian sediment trap. *Geomorphology*, **18,** 333–345.

Owen, P.R. (1964) Saltation of uniform grains in air. *J. Fluid Mechan.*, **20,** 225–242.

Rasmussen, K.R., Iversen, J.D. and Rautahemio, P. (1996) Saltation and wind–flow interaction in a variable slope wind tunnel. *Geomorphology*, **17,** 19–28.

Sweet, M.L. and Kocurek, G. (1990) An empirical model of aeolian dune lee-face airflow. *Sedimentology*, **37,** 1023–1038.

Taylor, P.A. and Gent, P.R. (1974) A model of atmospheric boundary layer flow above an isolated two-dimensional hill; an example of flow above gentle topography. *Boundary-Layer Meteorol.*, **7,** 349–362.

Tsoar, H. (1985) Profile analysis of sand dunes and their steady state significance. *Geografiska Annaler*, **67A**, 47–59.

Wiggs, G.F.S. (1993) Desert dune dynamics and the evaluation of shear velocity: an integrated approach. In: *The Dynamics and Environmental Context of Aeolian Sedimentary Systems* (Ed. by K. Pye), pp. 37–48. Geological Society, London.

Xu, D. and Taylor, P.A. (1992) A non-linear extension of the mixed spectral finite difference model for neutrally stratified turbulent flow over topography. *Boundary-Layer Meteorol.*, **59,** 177–186.

Manuscript received 14 May 1996; revision accepted 19 February 1997.